



## COMBUSTION CHAMBER DESIGN OF LIQUID-PROPELLANT ROCKET ENGINE OF 55kN POWERED BY ETHANOL AND LOX

Gabriel Costa Guerra Pereira

Pedro Teixeira Lacava

Instituto Tecnológico de Aeronáutica, Praça Marechal Eduardo Gomes, 50, São José dos Campos, SP, Brazil  
gpereira@ita.br, placava@ita.br

**Abstract.** This paper describes some aspects of the influence of ethanol use as fuel for propulsion of aerospace vehicles compared to kerosene use. A Russian method to calculate a liquid propellant rocket chamber is employed based on the chamber that belongs to the Russian-made kerosene engine 8D719, which has been in operation successfully for decades. By this way, the two chambers are confronted satisfactorily. The results prove that to obtain the same specific impulse using ethanol, it is necessary to increase the nozzle expansion area ratio significantly from 82 to 131. Therefore, the combustion chamber is 275mm longer in length and 181mm in outlet diameter. Considering that, the main differences between the two engines are due to the combustion chambers, the mass of the designed engine increases 3% when compared to the kerosene engine. Calculations have shown that the results are reasonable, but they need to be validated through experimental tests with prototypes.

**Keywords:** combustion chamber, liquid propulsion, aerospace engineering, ethanol.

### 1. INTRODUCTION

In the late 90s, there was an advance in the development of liquid propulsion rocket engines in Brazil. Currently, several activities in this area have been in development (Torres et al., 2009). To contribute to the Brazilian Space Program, a rocket engine combustion chamber fueled by ethanol and liquid oxygen was designed based on the chamber of the Russian engine 8D719.

To start a combustion chamber design, it is necessary to know the characteristics of the engine where the chamber will be integrated. The design requirements are based on the engine 8D719 parameters such as thrust and specific impulse in vacuum, chamber pressure, total propellant mass flow rate, as well as other settings which were established this way. In Tab. 1 the main parameters involved in the combustion chamber design are listed. The engine that contains the ethanol chamber is called L55.

Table 1. Main parameters of L55.

Parameters	Descriptions
Specific impulse in vacuum ( $I_s$ )	3600 m/s (theoretical)
Thrust in vacuum ( $F$ )	55 kN
Chamber pressure ( $P_{ch}$ )	5 MPa
Overall mass flow rate ( $\dot{m}$ )	16.5 kg/s
Mass ratio between dump cooling system and total propellants of chamber ( $\bar{m}_d$ )	0.035
Mass ratio between liquid-film cooling and total propellants of chamber ( $\bar{m}_l$ )	0.01

### 2. PROJECT DESCRIPTIONS AND PROCEDURES

The project was developed using the methodology described by Vassiliev et al. (1993). First, using the software Chemical Equilibrium with Applications (CEA), it is determined the mixing ratio and the expansion ratio necessary to achieve the specific impulse desired. The results are shown in Fig. 1.

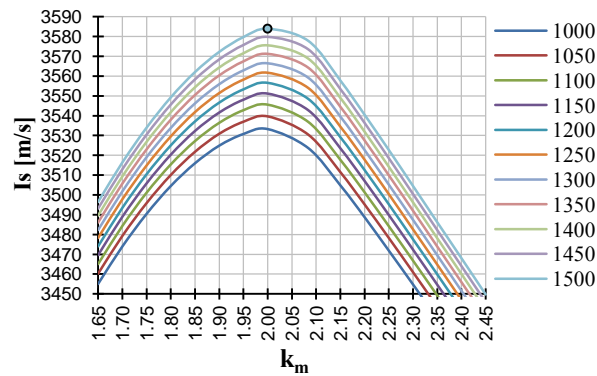


Figure 1. Performance curves as a function of mixing ratio.

The choice made by the expansion ratio 2.0 and mixing ratio 1500 that provides specific impulse near the desired (3600m/s) is highlighted in Fig. 1. This mixing ratio is set to the injectors and refined through iterative calculation using the following two equations, which relate the overall mixing ratio ( $k_m$ ) and the injector-mixing ratio ( $k_{m_i}$ ) as a function of the mixing ratio of the core ( $k_{m_c}$ ):

$$k_m = \frac{1 - \bar{m}_d - \bar{m}_i}{\frac{1}{k_{m_c}} + \bar{m}_d + \bar{m}_i} \quad (1)$$

$$k_{m_i} = k_{m_c} \left( 1 - \frac{\bar{m}_i}{\bar{m}_l - \bar{m}_d} \right) \quad (2)$$

Equation (1) and (2) are derived from the elementary expressions of the mixing ratio depending on the relative mass flow rates:

$$k_m = \frac{\bar{m}_o}{\bar{m}_f} \quad (3)$$

$$k_{m_i} = \frac{\bar{m}_o}{\bar{m}_f - \bar{m}_d} \quad (4)$$

$$k_{m_c} = \frac{\bar{m}_o}{\bar{m}_f - \bar{m}_d - \bar{m}_i} \quad (5)$$

where  $\bar{m}_o$  and  $\bar{m}_f$  are respectively the mass ratio of the oxidizer and the fuel depending on the total propellant mass of the chamber.

In Tab. 2, it is highlighted the definition of core mixing ratio (2.05), equivalent to the mixing ratio of the greater core specific impulse ( $I_{s_c}$ ) for an injector mixing ratio closer to 2.0 which was built with calculated parameters and obtained in the simulations iteratively.

Table 2. Mixing ratios definition.

$k_{m_c}$	$I_{s_c}$ [m/s]	$k_m$	$k_{m_i}$	$\bar{m}_f$	$\bar{m}_o$
1.98	3583	1.74	1.92	0.365	0.635
2.00	3584	1.75	1.94	0.363	0.637
2.05	3584	1.79	1.99	0.358	0.642
2.06	3582	1.80	2.00	0.357	0.643
2.10	3574	1.82	2.03	0.353	0.647

Then simulating the combustion chamber for expansion 1500 and mixture 1.99, the results displayed in Tab. 3 are obtained. The stoichiometric mixing ratio, obtained by CEA software, is 2.08.

Table 3. Simulation results of L55's combustion chamber.

Parameters	Results
Specific impulse ( $I_s$ )	3583 m/s
Nozzle expansion area ratio ( $\bar{A}_e$ )	131
Characteristic velocity ( $c^*$ )	1699 m/s
Thrust coefficient ( $C_f$ )	2.02
Sound velocity in the exit ( $a_e$ )	777.4 m/s
Mach number in the exit ( $M_e$ )	4.418

## 2.1 Chamber sizing

First, the areas of the critical cross section ( $A_{cr}$ ) and the outlet ( $A_e$ ) are calculated through Eq. (6) and (7), and, from them, their respective diameters,  $d_{cr}$  and  $d_e$ . The cylindrical region of chamber, where the actual combustion occurs, has the same dimensions as the reference motor chamber.

$$A_{cr} = \frac{c^* C_f}{P_{ch} I_s} \quad (6)$$

$$A_e = \bar{A}_e A_{cr} \quad (7)$$

The calculations performed regarding the dimensioning of the subsonic (convergent) region shown in Fig. 2 are described below.

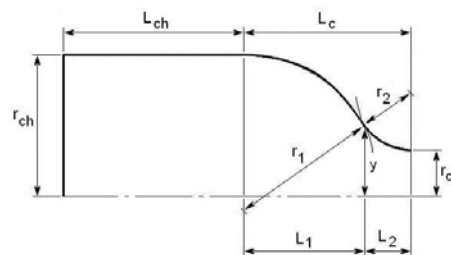


Figure 2. Profile of cylindrical and subsonic parts.

To determine the radius of the first curve of subsonic profile ( $r_1$ ), the definition of factor  $\bar{r}$  is required. Chose factor  $\bar{r}$  equal to 1.5 according to Tab. 4.

Table 4. Factor conditioned to the chamber pressure.

$P_{ch}$ [Mpa]	< 5	5 to 10	> 10
$\bar{r}$	1.0 to 1.5	1.5 to 2.0	2.0

So the radii of the first and second subsonic profile curves are defined by Eq. (8) and (9).

$$r_1 = \bar{r} r_{ch} \quad (8)$$

$$r_2 = d_{cr} \quad (9)$$

The longitudinal lengths related to these curves are calculated by Eq. (10), (11) and (12).

$$L_c = 0.5 d_{cr} \sqrt{(2 + \bar{r} \sqrt{\bar{A}_c})^2 - [(\bar{r} - 1)\sqrt{\bar{A}_c} + 3]^2} \quad (10)$$

where  $\bar{A}_c$  is the nozzle contraction area ratio, i.e. the ratio between the cross section areas of cylindrical and critical regions.

G. Pereira and P. Lacava  
Design of LRE Combustion Chamber

$$L_1 = \left(1 - \frac{L_2}{L_c}\right) L_c \quad (11)$$

$$L_2 = \frac{2}{2 + \rho \sqrt{A_c}} L_c \quad (12)$$

Already the radius  $y$  of the cross section shown in Fig. 2 is obtained by Eq. (13).

$$y = \left(\frac{L_2}{L_c} \sqrt{A_c} + \frac{L_1}{L_c}\right) r_{cr} \quad (13)$$

Made up afterward the calculation of the supersonic (divergent) profile exposed in Fig. 3

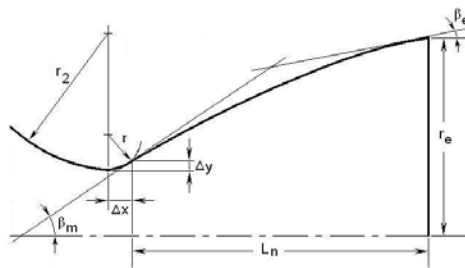


Figure 3. Profile of supersonic part.

Seconds Vassiliev et al. (1993), for  $d_e/d_{cr}$  equal to 11.5 have the following tabulated parameters,  $\beta_e$  equal to  $11^\circ$ ,  $\beta_m$   $42^\circ$ , and  $\bar{L}_n$  26.7. Assuming these values, it is calculated the longitudinal length of the nozzle ( $L_n$ ), the radius  $r$  of the beginning of the divergent profile, and the lengths  $\Delta x$  and  $\Delta y$  indicated in Fig. 3:

$$L_n = \bar{L}_n r_{cr} \quad (14)$$

$$r = 0.2 d_{cr} \quad (15)$$

$$\Delta x = r \sin(\beta_m) \quad (16)$$

$$\Delta y = r[1 - \cos(\beta_m)] \quad (17)$$

Therefore the total longitudinal length of the chamber ( $L_t$ ) is achieved by:

$$L_t = L_{ch} + L_c + \Delta x + L_n \quad (18)$$

## 2.2 Regenerative cooling

The heat of combustion gas products is conveyed to the chamber casing by convection and radiation, and it is often necessary to cool it to maintain the physical integrity of the material which is manufactured, mainly in the critical region. The regenerative cooling method is the most used in the liquid rocket engines, and, to design this system it is essential to determine the heat flow of combustion gases to the chamber wall. Therefore, it is necessary to know the temperature curve as a function of the mixing ratios to the pressure chamber, which is obtained by CEA and displayed in Fig. 4.

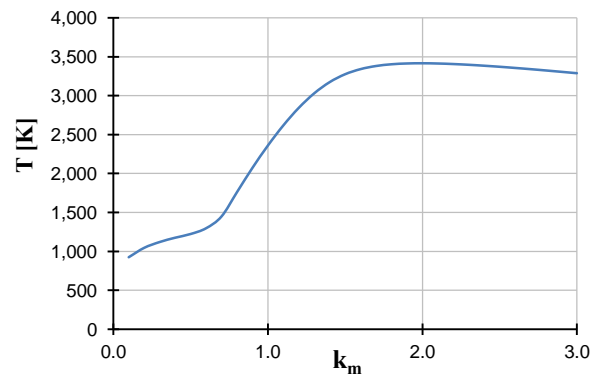


Figure 4. Temperature curve as function of mixture ratio.

Using a CAD software, we draw up the camera and slice it in twenty cross sections registering their distances to the injector plate. And through the CEA, it is possible to obtain the Mach number and the speed of sound in each section, parameters needed to heat flow calculations.

The convection heat flow from the combustion gases to the chamber wall is determined by:

$$q_c = \frac{B(1-w_i^2)P_{ch}^{0,85}S}{\bar{d}_i^{1,82}d_{cr}^{0,15}P_r^{0,58}} \quad (19)$$

where  $B$  is the damping coefficient of the heat flow determined according to Tab. 5;  $w_i$  is the dimensionless velocity;  $\bar{d}_i$  is the ratio between the diameter of any cross section and critical diameter;  $P_r$  is the Prandtl number, and  $S$  is a complex of thermal-physics parameters that depends on the mixing ratio in the region closest to wall, and it is obtained by Eq. (20).

$$S = \frac{(h-h_w)\nu_{1000}^{0,15}T_o^{0,425}}{R^{0,425}(T_{og}+T_{wg})^{0,595}(3T_o+T_{wg})^{0,15}} \quad (20)$$

there  $h$  the enthalpy of gases;  $h_w$  the enthalpy to temperature of chamber wall;  $\nu_{1000}$  the dynamic viscosity of gas to temperature 1000K;  $R$  the combustion gas constant;  $T_o$  the stagnation temperature of combustion products;  $T_{og}$  the temperature in the region closest to wall;  $T_{wg}$  the wall temperature on the face in contact with the gas.

Table 5. Coefficient linked to the temperature ratio.

$T_{wg}/T_o$	0.1	0.2	0.3	0.4	0.5
$B$	8.45	8.48	8.53	8.59	8.67

Analyzing the two most pertinent products of combustion, carbon dioxide and water vapor, the calculation of radiation heat flow is done. To determine each component mentioned in the heat flow, Eq. (21) and (22) are used.

$$q_{rCO_2} = 4.0705(1.02 * 10^{-5}p_{CO_2})^{1/3}L_i^{1/3} \left[ \left( \frac{T_o}{100} \right)^{3,5} - \left( \frac{T_{wg}}{100} \right)^{3,5} \right] \quad (21)$$

$$q_{rH_2O} = 4.0705(1.02 * 10^{-5}p_{H_2O})^{4/5}L_i^{3/5} \left[ \left( \frac{T_o}{100} \right)^3 - \left( \frac{T_{wg}}{100} \right)^3 \right] \quad (22)$$

where  $p_{CO_2}$  and  $p_{H_2O}$  are the partial pressures of carbon dioxide and water vapor in a section and they are obtained by CEA;  $L_i$  is the equivalent length and it is obtained by Tab. 6.

Table 6. Equivalent length.

$L_{ch}/d_{ch}$	1.0	1.5	2.5
$L_i$	$0.6 d_i$	$0.75 d_i$	$0.85 d_i$

Thus the radiation heat flow is gotten by summing the contribution of each gas component:

$$q_r = q_{r_{CO_2}} + q_{r_{H_2O}} \quad (23)$$

Once acknowledged the total heat flow ( $q_t$ ), equivalent to the sum of convection and radiation heat flows across the chamber, the sizing of damp cooling system is started. This system is designed with longitudinal channels of rectangular section (Fig. 5), used to increase the heat exchange surface and thereby increasing the cooling efficiency. The liquid fuel goes through the channels before being injected into the combustion chamber, cooling it. The efficiency is a function of the channel geometry, the thermal-physics properties of the coolant and the thermal properties of the channel material. These channels are machined into the inner-shell that is itself welded to the outer-shell, whose function is to increase the mechanical strength of the chamber. This cooling system has advantages such as higher reliability and lower cost of construction, besides using simple manufacturing processes (Almeida et al., 1999).

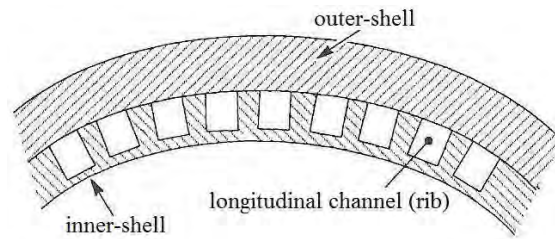


Figure 5. Damp cooling scheme.

Figure 6 shows the limits suggested by the literature (Zinchuk, 2008) for the design of the rectangular section of the longitudinal channels (ribs) by which the coolant goes through. These ranges are based on experience improved in the development of this system and also encourage manufacturing processes.

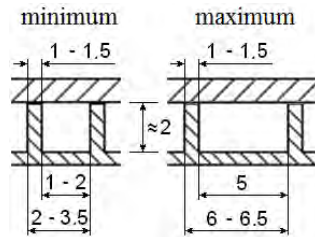


Figure 6. Rib dimensions [mm].

Initially, it is adopted the rib thickness ( $\delta_r$ ) between 1 and 1.5mm, the pitch ( $t_r$ ) from 2 to 6.5mm, and rib height ( $h_r$ ) equivalent to 2mm. Then, it is calculated the number of ribs ( $n_r$ ) obtained in the cylindrical, subsonic and supersonic regions of the chamber through Eq. (24).

$$n_r = \frac{\pi (d_i + 2 \delta_{in})}{t_r} \quad (24)$$

where  $\delta_{in}$  is the inner-shell thickness.

After calculating the number of channels and obtaining the steps in the pre-defined sections located in the subsonic region, especially in the throat, it shall be considered the minimum recommended limits, because otherwise their ribs may be obstructed during the welding process between the inner and outer-shell. It should also be checked the ribs in the supersonic region, since the diameters of the cross sections increase considerably in this region. It is not recommended that the maximum pitch ( $t_{r_{max}}$ ) exceed 6.5mm to minimize the occurrence of deformations in the shells (Zinchuk, 2008), because the ribs also function as beams. See Eq. (25). If this amount is exceeded, ribs should be added to reduce the intermediate step in the respective sections.

$$t_{r_{max}} = \frac{\pi (d_i + 2 \delta_{in})}{n_r} \leq 6.5\text{mm} \quad (25)$$

Using CAD software we obtain the profile lengths ( $\Delta x_i$ ) and the revolution areas ( $\Delta S_i$ ), arranged in Fig. 7, for the same twenty cross sections used in the calculation of heat flow from combustion gases to the chamber wall.

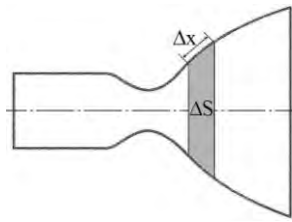


Figure 7. Scheme of a profile length and a revolution area between two sections.

The liquid is introduced into the outlet section of the chamber and its temperature increases along the damp cooling system until the end of the cylindrical region. Then, it is injected into the combustion chamber. To calculate the heat flow from the heated wall to the coolant, first it is necessary to determine the liquid temperature variation during the cooling of chamber:

$$\Delta T_i = \frac{\Delta S_i}{\dot{m}_l c_i} \left( \frac{q_{t_i} + q_{t_{i+1}}}{2} \right) \quad (26)$$

where  $\dot{m}_l$  is the mass flow rate of the coolant and  $c_i$  is the specific heat of the coolant (fuel) to the site temperature of the section.

It is calculated through Eq. (27) the coolant temperatures in each section considering the inlet temperature of the cooling system equal to 298K.

$$T_i = T_{i-1} + \Delta T_i \quad (27)$$

It is worth noting that the calculation of the coolant temperature along the damp cooling system is made in the opposite direction of the combustion gas flow. Likewise, it is calculated the coolant temperature in the first section ( $T_{i=20}$ ) adopting the coolant specific heat at the initial temperature (298K). Taking the first approach of temperature for this section, the value of specific heat is updated for the first approached temperature in Eq. (26) and the second approximation is done for  $T_{i=20}$  by Eq. (27). This procedure is repeated until the specific heat  $c_{i=20}$  reaches temperature  $T_{i=20}$ . The same happens to the other cross sections.

To determine the heat flow from the wall heated by gases to the coolant, it is estimated the inner-shell temperatures on the side in contact with the coolant ( $T_{wl}$ ).

$$T_{wl} = T_{wg} - \frac{\delta_{in}}{\lambda_{in}} q_t \quad (28)$$

where  $\lambda_{in}$  is the thermal conductivity of the inner-shell material.

The heat transfer coefficient from the inner-shell to the coolant may be determined by Eq. (29).

$$\alpha_l = 0,023 \frac{c^{0,4} \lambda^{0,6} (\rho w_l)^{0,8}}{d_h^{0,2} \mu^{0,4}} \quad (29)$$

where  $c$  (specific heat),  $\lambda$  (thermal conductivity),  $\rho$  (density) e  $\mu$  (viscosity) are the proprieties of the coolant (fuel) to section temperature;  $w_l$  is the fuel speed in a section and  $d_h$  is the hydraulic diameter obtained by Eq. (30).

$$d_h = 2 h_r \left( \frac{t_r - \delta_r}{t_r - \delta_r + h_r} \right) \quad (30)$$

Finally, the heat flow from the wall to the liquid may be calculated by Eq. (31).

$$q_l = \alpha_l (T_{wl} - T_l) \quad (31)$$

there  $T_l = T_i$ .

### 2.3 Load carrying capacity

The load carrying capacity of the chamber casing with connected shells can be estimated by the value of the limiting gas pressure. To determine the limiting gas pressure it is necessary to construct the curve that expresses the relationship between the chamber pressure and its radial elongation under the combined loading of pressure and temperature. The

limiting gas pressure is the pressure value in which a small increment over it corresponds to a large increase in radial elongation of the shells by developing plastic deformations in both shells.

Copper alloy UNS C18200 was used for inner-shell and the stainless steel AISI/SAE 304 for outer-shell. From the force balance equations, it is possible to write the equation of the gas pressure ( $P_g$ ) and the mechanical strain ( $\varepsilon$ ), given by Eq. (32) and (33).

$$P_g = \frac{\delta_{in}\sigma_{in} + \delta_{out}\sigma_{out}}{r_{ch}} \quad (32)$$

$$\varepsilon = \varepsilon_t - \alpha T \quad (33)$$

where  $\sigma_{in}$  e  $\sigma_{out}$  are the stresses in inner and outer-shell materials for calculated temperatures;  $\delta_{out}$  the outer-shell thickness;  $r_{ch}$  the chamber radius;  $\varepsilon_t$  the total strain,  $\alpha$  the coefficient of thermal expansion; and  $T$  the material temperature.

Assuming the total strain equals the ratio of radial elongation by chamber radius and knowing the thermal expansion shell temperature, it's possible to obtain the mechanical strain. Calculating the mechanical strain on each shell for different values of radial elongation, the respective stresses are obtained across the stress-strain curve of the material, and thus it is possible to determine gas pressures. The safety factor ( $n$ ) is obtained by the ratio between the limiting gas pressure ( $P_{gu}$ ) and the pressure chamber, respecting the margin from 1.2 to 1.5. If it is outside this range, it is recommended to change the thickness of the outer-shell (Almeida et al., 1999).

$$n = \frac{P_{gu}}{P_{ch}} \quad (34)$$

### 3. RESULTS AND DISCUSSIONS

In Tab. 7, it is presented a summary of the main results achieved by comparing them with the reference engine.

Table 7. Engine comparatives.

Parameters	L55	8D719
Propellants	Ethanol + LOx	Kerosene + LOx
Thrust	55 kN	54 kN
Chamber pressure	5.2 MPa	5.2 MPa
Exit pressure	3.5 kPa	5.5 kPa
Expansion ratio	1500	950
Fuel mass flow rate	5.9 kg/s	5.0 kg/s
Oxidizer mass flow rate	10.6 kg/s	11.5 kg/s
Mixture ratio	1.79	2.32
Specific impulse	3222 m/s	3249 m/s
Characteristic velocity	1676 m/s	1762 m/s
Thrust coefficient	2.02	1.94
Expansion area ratio	131.0	82.2
Chamber diameter	180 mm	180 mm
Critical diameter	82.8 mm	84.5 mm
Exit diameter	947 mm	766 mm
Chamber length	190 mm	190 mm
Nozzle length	1103 mm	861 mm
Total length	1442 mm	1167 mm

It was noticed that the L55's chamber is 275mm longer and its exit diameter is 181mm higher than the chamber of 8D719. This is due to the application of a considerably higher expansion ratio compared to the reference engine in order to compensate the loss of the specific impulse from the use of ethanol instead of kerosene, which occurs because ethanol has either a heating value lesser than kerosene or a smaller quantity of released energy per unit mass during combustion.

Figure 8 shows the curves of convection and radiation heat flow, and also the total heat flow from the combustion gases to the chamber wall. It was observed that the convection heat flow increased significantly from the beginning of the subsonic region until it reaches the maximum value around 10MW/m<sup>2</sup> in the critical section, and then decreased gradually with the acceleration of gases until the nozzle exit. This result is expected, since the critical section has the smallest cross-section area of the chamber. The radiation heat flow was higher (1.6MW/m<sup>2</sup>) in the cylindrical region

and began to decrease in the subsonic region until the chamber exit. This occurs because the operating pressure decreases along the chamber and consequently the partial pressures of carbon dioxide and water vapor. The peak of total heat flow equivalent to 11MW/m<sup>2</sup> was attained in the throat, and its curve behaved similarly the convection heat flow under little influence of radiation from the combustion.

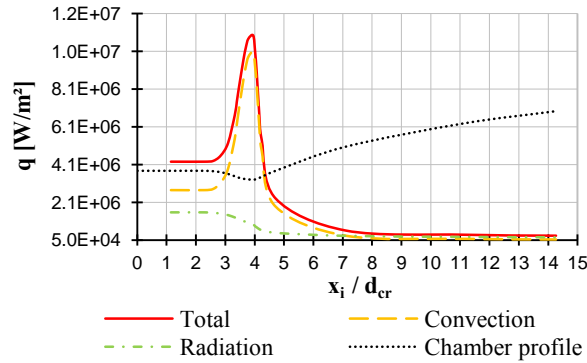


Figure 8. Heat flow from combustion product gases to inner-shell.

Figure 9 displays the temperature curve of fuel used in the regenerative cooling. It is recommended that this temperature does not exceed the saturation temperature ( $T_s$ ) at the cooling system pressure or the decomposition point of the fuel (Zinchuk, 2008). It was observed that the coolant temperature increased gradually until critical region, where it had an abrupt increase because the high rates of heat transfer in this region, reaching 485K in the cooling system outlet.

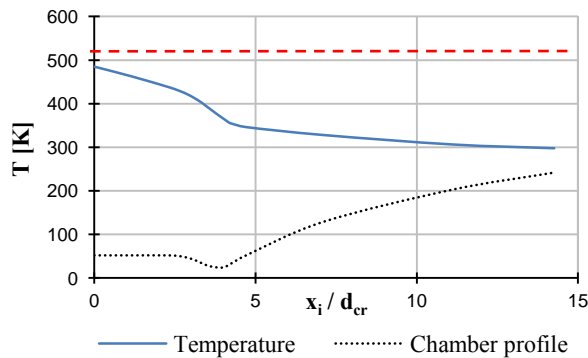


Figure 9. Coolant temperature.

The gas pressure curve obtained is shown in Fig. 10. The gas pressures were calculated for different strains at average temperatures of 700 and 400K for inner and outer-shell respectively. In graphic, it is highlighted the limiting gas pressure obtained by the tangent to the curve that crosses the origin of the Cartesian plane. This point determines the onset of permanent deformations, which may compromise the equipment safety.

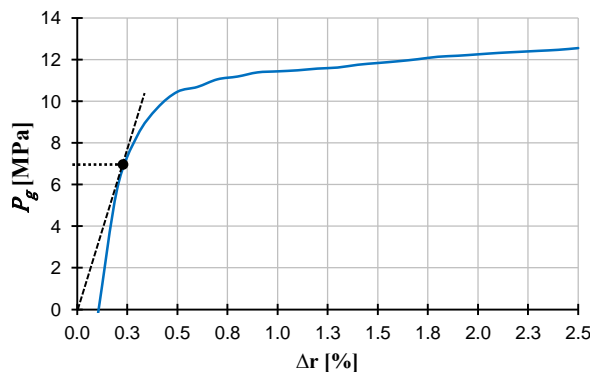


Figure 10: Gas pressure as a function of radial elongation

G. Pereira and P. Lacava  
Design of LRE Combustion Chamber

#### 4. CONCLUSION

The applied methodology showed a way to design a combustion chamber of liquid rocket engine. Through this procedure it was possible to perform the chamber geometric dimensioning of double wall with internal cooling channels, determine the heat flows along its contour and estimate its load carrying capacity, yielding important information for finite element analysis, essential for the project validation. The cooling system is extremely important because of the high temperatures that the chamber is subjected to during operation.

According to the atlas of Russian engines (Ordzhonikidze, 1969), engine 8D719 weighs about 121kg and its camera approximately 6kg. It is estimated that the mass of L55's chamber is 10kg, an increase of 67% compared to 8D719. Whereas the differences between these engines are limited to the chamber, the mass difference between them is likely to be 2.5%, although the reported weight for the chamber of reference engine is doubtful. However, there is an aggravating point caused by an increase of 4.7% in the volume of the tanks of propellant due to the difference between the density of fuels and the propellant mass flow rates. Probably, it becomes advantageous to increase the expansion ratio to compensate the thrust loss due to the lesser heating value of ethanol in relation to kerosene, instead of increasing the mass flow rates of the propellant.

Even raising the expansion ratio from 950 to 1500, the mass difference between the two chambers is viable for the application. Due to its higher heating value, kerosene shows a fuel more attractive from the standpoint of mass saving, since the average boarded kilogram considering placed payloads into orbit is on the order of US\$40,000.00, and pondering yet a complete space mission cost, this figure might be much higher, around US\$260,000.00 (James, 1996). Therefore, the lesser the aggregate mass to the engine is, the greater the availability for payloads. However, the use of ethanol has advantages such as low toxicity, safer operation compared to kerosene. In addition, it is obtained from renewable sources, and Brazil is the world's largest producer of ethanol derived from sugarcane.

#### 5. REFERENCES

- Almeida, D.S., Shimote, W.K. and Niwa, M. "Selection of Materials for Combustion Chamber of Liquid-Propellant Rocket Engine". In *Proceedings of the 20<sup>th</sup> Brazilian Congress of Mechanical Engineering - COBEM1999*. Gramado, Brazil.
- Chemical Equilibrium with Applications. 7 Nov. 2012 <[www.grc.nasa.gov/WWW/CEAWeb/ceaWhat.htm](http://www.grc.nasa.gov/WWW/CEAWeb/ceaWhat.htm)>.
- Ordzhonikidze, S., 1969. *Private Communication*. Moscow Aviation Institute, Moscow.
- Pereira, G.C.G., 2011. *Combustion Chamber Design of Liquid-Propellant Rocket Engine of 55kN Powered by Ethanol and LOX*. Master dissertation, Technological Institute of Aeronautics, São José dos Campos.
- Torres, M.F.C.; Almeida, D.S.; Krishna, Y.S.R., Silva, L.A.; Shimote, W.K. "Liquid Propulsion at IAE: Vision of the activities and future perspectives". *Journal of Aerospace Technology and Management - JATM*. 22 May 2009.
- Vassiliev, A.P.; Kudriavtsev, V.M.; Kusnetsov, V.A.; Kurpatenkov, V.D.; Obelnitski, A.M.; Polaev, V.M.; Poluan B.A. *Fundamentals of Theory and Calculation of Liquid-Propellant Rocket Engines*. Visshaia Shcola, Moscow. (In Russian)
- Wertz, J.R. and Larson, W.J., 1996. *Reducing Space Mission Cost (Space Technology Library)*. Springer, London.
- Zinchuk, A.A., 2008. *Private Communication*. Technological Institute of Aeronautics, São José dos Campos.

#### 6. RESPONSIBILITY NOTICE

The authors are the only responsible for the printed material included in this paper.